INDONESIAN JOURNAL ON GEOSCIENCE
Geological Agency
Ministry of Energy and Mineral Resources

Journal homepage: http://ijog.geologi.esdm.go.id
ISSN 2355-9314, e-ISSN 2355-9306

Terrestrial Laser Scanner (TLS) Measurement in A Volcanic Area: Detection of Error Source and Scanned Object Intensity

Nia Haerani[1], Hasanuddin Z. Abidin[2], Surono[1], and Dudy D. Wijaya[2]

[1]Center for Volcanology and Geological Hazard Mitigation, Geological Agency
Jln. Diponegoro No. 57 Bandung 40122 - West Java, Indonesia
[2]Geodetic Engineering, Faculty of Earth Sciences, - Bandung Institute of Technology
Jln. Ganesha No. 10 Bandung 40123 - West Java, Indonesia

Corresponding author: nia.haerani@gmail.com
Manuscript received: April, 10, 2017; revised: june, 5, 2018;
approved: January, 20, 2020; available online: July, 6, 2020

Abstract - The purpose of the study of Terrestrial Laser Scanner (TLS) application in an active volcanic crater is to detect the influence of gas emission and local atmospheric change into the accuracy of measurement.The measurement was conducted at Papandayan Volcano crater, along with the local temperature, humidity, and air pressure (*thp*). The measured target located near a gas emission hole gives a significant fluctuative range due to possible false return by gas particles. The refraction index was calculated using *thp* data. Two correction models were applied: velocity-geometry and atmospheric delay correction. The atmospheric delay correction gives a more reliable result, however their refraction index calculation does not accomodate specific volcanic gas yet. An intensity map obtained from TLS can also be used for rock segmentation. An experiment from some types of volcanic rocks shows that the intensity value is influenced by a weathering degree of rock outcrops. Rock segmentation using TLS intensity data for fresh outcrops is relatively easier, while for weathered rocks it still needs a field check for validation. The temperature of volcanic rocks also contributes to the intensity value. It is found that the intensity increases along with the temperature of rock.

Keywords: laser scanner, gas emission, correction model, intensity

How to cite this article:
Haerani, N., Abidin, H.Z,. Surono, and Wijaya, D.D., 2020. Terrestrial Laser Scanner (TLS) Measurement in A Volcanic Area: Detection of Error Source and Scanned Object Intensity. *Indonesian Journal on Geoscience*, 7 (2), p.179-200. DOI: 10.17014/ijog.7.2.179-200

Introduction

Terrestrial laser scanning is a method of surface sampling using laser technology. Scanning with laser has the objective to collect visual data of an object that includes the shape and colour. Data collected can then be used for 3D reconstruction with the help of various types of software. Scanning with laser has advantages compared with conventional methods (*e.g.* tacheometry, EDM, photogrammetry), in terms of higher accuracy and less time consume during a field survey (Pesci *et al*., 2008). In addition, laser scanning results can record a huge number of points named point clouds that contain data of *x, y, z (RGB, I*), with *xyz* is the position of an object, *I* is the intensity and *RGB* is the colour of an object. TLS can reconstruct digital model of an object precisely with the accuracy up to submillimeter (Colombo and Marana, 2010). TLS method is able to describe the condition of outcrop/surface closer to the actual condition, both in terms of geometry and spatial with excellent accuracy. Therefore, it can be applied for deformation monitoring (Waggot *et al*., 2005 and Tsakiri *et al*., 2006).

In addition to these advantages, the TLS has error sources that can affect the measurement results and can reduce the accuracy. These errors are related to four sources, namely: equipment, methodology of data collection, environmental, and scanned objects (Quintero *et al*., 2008; Reshetyuk, 2009).

A research to determine the error source from instrument has been done by Litchi *et al*. (2006) and Reshetyuk (2009). The two researchers have conducted modeling and calibration using Faro 880, Callidus CP 3200, Leica HDS 3000, and the Leica Scan Station. In addition, to examine the error originating from the instrument, Reshetyuk (2009) also examined the error source derived from the methodology, particularly in geo-referencing process.

Hunter *et al*. (2003), Jones (2007), Pesci *et al*. (2008), Bonforte *et al*. (2011), Vidyan *et al*. (2013), and Jones *et al.* (2015) had apllied TLS measurement in a volcanic area, but only limited in deformation and slope stability monitoring, and 3D topography modeling. The researchers did not discuss the performance, nor the accuracy of measurement data in detail. They also did not discuss the error sources of volcanic environments, especially the ones associated with the activity of volcanic gases and local atmospheric conditions.

Rueger (1990) had written speed and geometry correction formula for measurement by Electro-optic Distance Meter (EDM) which used visible waves (optical). Meanwhile, Wijaya (2010) had formulated a unified zenith delay correction models for satellite-based distance measurement using micro (GNSS/VLBI) and optical (SLR) waves. Therefore, a correction model of these two researchers was tried to be applied for TLS measurement results, in other words to use or test the old concept with new technology.

A research on the response of scanned object, in this case expressed in terms of intensity, had been conducted by Litchi and Harvey (2002), Pfeifer *et al*. (2007), and Voegtle *et al*. (2008).The three researchers scanned artificial objects, metal, and some rocks which were not of volcanic eruption product. Their study emphasizes on intensity values and their relation to the distance and angle of the scan. In this research, the focus is on a volcanic rock, especially the relation between volcanic rock surface properties (including colour, surface texture, crystal content, pores, temperature, and impurities) with intensity values. This study of rock intensity is a preliminary quantification. Implications of the intensity value to distance accuracy are not described in detail, since they require another parameter that should be tested.

Error Source of TLS in Volcano Environment

Error sources within volcanic environment is very complex due to several factors that occur simultanously and they can affect the measurement results, as illustrated in Figures 1 and 2. Sources of error associated with wave dispersion are due to separation of spectrum frequency of laser beam on inhomogeneous medium/atmosphere, in this case the medium containing particles of volcanic gases.

Local weather in an active volcanic crater tends to be fluctuative quickly, and will contribute in reducing the accuracy of measurement. Hunter *et al.* (2002) has applied TLS in Mount Etna and found that TLS has limitation to penetrate volcanic fog. Radiometric contribution has to be considered.

Ingensand (2006) offended correlation between scanned object factors and measurement results. He states that in theory, the error of the coordinate system (S_{xyz}) from a point cloud is a function of:

- distance (D); which correlates with atmospheric parameters
- reflectivity of the object; affects the signal to noise ratio (SNR)
- ambient light; affect SNR
- angle of incidence ray (θ)
- wavelength; correlated with surface roughness of rock and produce spots/speckles
- (white noise)
- colour of the object surface
- object surface roughness
- geometry of the object; could lead to multipath effects

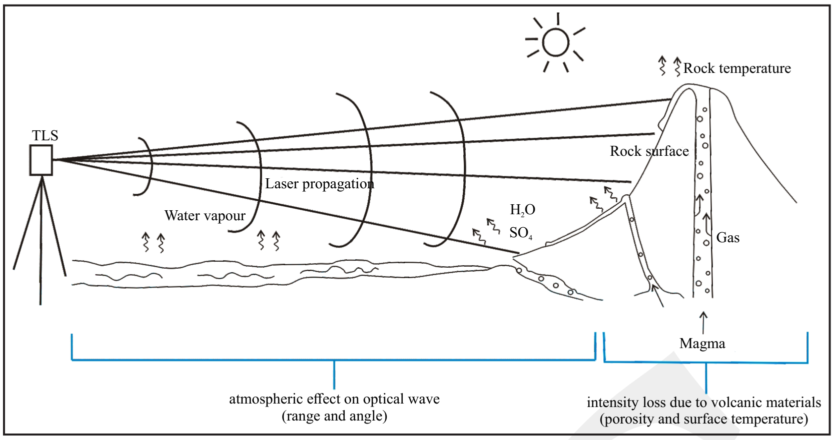

Figure 1. Illustration of possible error budgets obtained in an active volcanic area (Haerani, 2016).

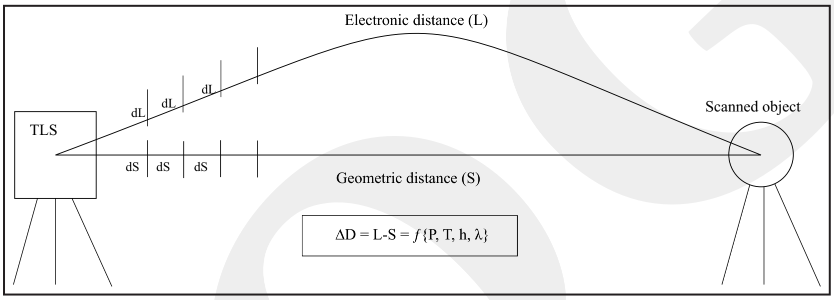

Figure 2. Simple mathematical illustration to describe the correlation of volcanic environment effect into TLS measurement (Haerani, 2016).

Bonforte *et al*. (2011) stated that volcanic rocks of black porous lava had poor reflectivity characteristics. It means that the nature and types of objects have different responses to TLS. Boehler and Marbs (2002) said that TLS measurements in areas of dust or water vapour/gas could cause an error resembles the edge effect. This is because laser propagation velocity changes due to variations in temperature and pressure. Edge effects occur if part of the object edge is reflected, while the other part was behind or around the scanned object. Even if there are no other objects in the vicinity, the laser will not be reflected at all.

Grantham *et al*. (1997) who conducted a study on the atmospheric effects into TLS measurement results discovered a phenomenon of dropout pixels, a condition in which the laser pulse is too weak to trigger a receiver, so the record is zero or maximum value of the pixel. This phenomenon is associated with laser attenuation. Grantham *et al*. (1997) also concluded the presence of false return phenomenon, which were laser dispersed by rain water droplets, aerosols, water vapour, or dust particles suspended in the air, that was strong enough to trigger the receiver. Most of transmitted laser energy is reflected by the particles and partly by the object surface. These conditions build up laser pulses (multiple return pulses) and contaminate generated data, thus complicate object scanned identification process.

Material and Methods

TLS Acquisition in A Volcanic Crater Area

TLS range measurement was conducted at Papandayan Volcano, West Java, using Leica Scan Station C10. Three planar targets were placed near a gas emission hole at some distances: ± 50 m (target A), ±100 m (target B), and ±150 m (target C). During the measurement, volcanic gas emission often crossed in front or near the target, mostly to target A.

Each target was measured fifty times, but on target C~150 m the measurements can only be done twenty-one times due to the instrument problem. The specifications of the instrument could actually reach optimal distances up to 300 m, but the volcanic crater conditions with a lot of gas emission obstructed the view between TLS and the target. During the distance measurement, weather data recording *thp* (air temperature, relative humidity, and air pressure) also performed automaticsensor (TNDD TR-73U) every 5 seconds. Two *thp* sensors were placed on TLS (base) and in the target (rover). At measurement of target B~100 m, a gap occured ± 60 minutes at rover sensor due to data downloading process.

Intensity Value Experiment

A simple experiment to determine the intensity of a volcanic rock was performed by scanning some examples of volcanics (volcanic bombs, lava, and pumice) with various surface properties. Volcanic rocks selected in this experiment are a common type of volcanic rock in Indonesia (andesitic-basaltic type).

The intensity measurements were carried out inside a room with a distance of 3.6 m, with different lighting (dark and bright light conditions). Reshetyuk (2006) concluded that for TLS type Leica HDS 3000, there was no systematic differences in ambient lighting. This experiments also did not perform a scan from several different distances, because the addition of the distance would reduce the intensity values (Pfeiffer *et al*., 2008). Volcanic rocks scanned are in dry conditions to avoid the water particles that can serve as a dominant reflector (water film). In this experiment, pure intensity values derived from the rock surface were expected to be obtained. Point cloud used Cyclone v.7 for object filtering process, converted to ASCII format. Plotting and normalization of intensity values were done by using Matlab software. Scanning process used a high resolution setting with air temperature at the time of scanning was 25.9 - 26°C; 59 - 61% of relative humidity, and 933.3 m bar of air pressure.

In order to determine the relationship between an intensity value and object temperature, a scanning process was performed at some areas of Papandayan volcanic crater, to obtain an intensity map. Some parts of point clouds on the intensity-map was sampled and converted to *ptx* format for viewing the intensity value, then correlated with the estimated temperature value obtained with a thermal camera. The type of thermal camera used is FLIR T-440.

Calculation of Refraction Index

A calculation for refractivity of wet air component (consisting of dry air and water vapour) in some standard conditions was proposed by Ciddor (1996). He also calculated the density of each component relative to the total density at standard conditions. The standard refractivity value was then multiplied by the value of the relative density to get a partial refractivity value, and then the results of each component were combined. He also combined multiple equations to calculate the refractive index of Barrels and Sears (1939), Erickson (1962), Edlen (1966), Owens (1967), Peck and Reeder (1972), Birch and Downs (1994), and Hou and Thalmann (1994),

Input data used in the calculation of the refractive index include: wavelength (γ), air temperature (°C), air pressure (P, Pascal), the partial pressure of water vapour (P_w, Pascal), and the CO_2 content (x_c, ppm). The density of dry air component (ρ_{ds}) is calculated at 15°C temperature, pressure 101325 Pa, and $x_w = 0$ ($x_w = e/P$ is the molar fraction of water vapour in moist air). The density of pure water vapour (ρ_{vs}) is calculated at 20°C, 1333 Pa, $x_w = 1$. The formulation by Ciddor (1996) was carried out through several stages of the calculation. In this calculation, some constants used are as follows:

1. Constans for standard phase calculation and refractivity group of dry air component: $k_0 =$ 238.0185 μm^{-2}; $k_1 =$ 5792105 μm^{-2}; $k_2 =$ 57.362 μm^{-2}; $k_3 =$ 167917 μm^{-2}.
2. Constans for standard phase calculation and refractivity group of water vapour component:

w_0 = 295.235 µm^{-2}; w_1 = 2.6422 µm^{-2}; w_2 = -0.032380 µm^{-4}; w_3 = 0.004028 µm^{-6}.

3. Constants for svp (saturation vapour pressure) calculation: A = 1.2378847 x 10^{-5} K^{-2}; B = -1.9121316 x 10^{-2} K^{-1}; C = 33.93711047; D = -6.3431645 x 10^{3} K.
4. Factorial number to enhance water vapour: α = 1.00062; β = 3.14 x 10^{-8} Pa^{-1}; γ = 5.6 x 10^{-7} °C^{-2}.
5. Compresibility calculation uses: $Z = 1 - (p/T)[a_0 + a_1 t + a_2 t^2 + (b_0 + b_1 t)x_w + (c_0 + c_1 t)x_w^2] + (p/T)^2(d + ex_w^2)$

with:
a_0 = 1.58123 x 10^{-6} K Pa^{-1};
a_1 = -2.9331 x 10^{-8} K Pa^{-1};
a_2 = 1.1043 x 10^{-10} K^{-1} Pa^{-1};
b_0 = 5.707 x 10^{-6} K Pa^{-1};
b_1 = -2.051 x 10^{-8} Pa^{-1};
c_0 = 1.9898 x 10^{-4} K Pa^{-1};
c_1 = -2.376 x 10^{-6} Pa^{-1};
d = 1.83 x 10^{-11} K^{2} Pa^{-2};
e = -0.765 x 10^{-8} K ^{2}Pa^{-2}.

Calculation from Ciddor (1996) produces a refractive index that has encompassed all known factors (except oil contamination of the atmosphere as vapour/liquid water and the effects of absorption). In addition, these calculations have included all of physical parameters and units, as well as valid for all atmospheric conditions and a wave length between 350 to 1,300 nm.

Velocity and Geometry Correction (Rueger, 1990)

As mentioned before, in this study, a TLS Leica ScanStation C10 was used, which had Time of Flight (TOF) measurement principle. The distance measurement can be formulated as follow:

$$2d = c\,\Delta t' = c(t_R - t_E) \quad \text{.................................} (1)$$

Where:
d = distance displayed in TLS
c = velocity of light in a vacuum
Δt' = measured 'flight' time of the signal to the target and back
t_E = time of departure of pulse
t_R = time of arrival of returning pulse

Assuming that velocity of light in a normal medium (air) is known, then velocity of light propagation can be calculated if refraction index of air and velocity of light in a vacuum is known:

$$c = \frac{c_o}{n} \quad \text{..} (2)$$

Where:
n = refraction index of medium
c_o = velocity of light in a vacuum
c = velocity of light in medium

Formula (1) shows that distance accuracy (d) relies strongly on TOF accuracy (Δt'). Substitution of formula (2) to (1) forms equation as follow:

$$d' = \frac{c_o}{n_{REF}} \frac{\Delta t'}{2} \quad \text{..} (3)$$

Where:
d' = distance displayed on instrument
c_o = velocity of light in vacuum
Δt' = measured 'flight' time of the signal to the target and back
n_{REF} = reference refractive index of the instrument

Reference refractive index (n_{REF}) is defined as follow:

$$n_{REF} == \frac{c_o}{\lambda_{MOD} f_{MOD}} \quad \frac{c_o}{2U f_{MOD}} \quad \text{.....................} (4)$$

Where:
λ_{MOD} = constant modulation wavelength of instrument
f_{MOD} = constant modulation frequency of instrument
U = unit length of instrument, it is half of$_{MOD}$

After several steps (Rueger, 1990), K1 can be derived and written as:

$$K1 = -d'\left(n_{REF} - n\right) \text{ .... (5)}$$

Distance corrected (d) expressed becomes:

$$d = d' + d'(n_{REF} - n) \text{ .... (6)}$$

$$d = d' + K1 \text{ .... (7)}$$

2nd velocity correction can be calculated using equation as follows:

$$K2 = -d'\Delta \text{ .... (8)}$$

or

$$K2 = -(k - k^2)\frac{d'^3}{12R^2} \text{ .... (9)}$$

Where:
K2 = 2nd velocity correction
k = coefficient of refraction
d' = measured distance
R = mean radius of curvature of the spheroid

$$k = \frac{curvatureofraypath}{curvatureofsphreroid} = \frac{1/r}{1/R} = \frac{R}{r} \text{ .... (10)}$$

$$r = \frac{R}{k} \text{ .... (11)}$$

$$\frac{1}{r} = -\sin z \frac{1}{n}\left(\frac{dn}{dh}\right) \text{ .... (12)}$$

Where:
(dn/dh) is vertical gradient of refractive index of air, and z is the angle between the direction of gradient of refractive index and the tangent to wave path.

Geometric correction (K3) obtained used equation as follow:

$$K_3 = \frac{d_2^{\,3}}{24r^2} - k^2 \frac{d_1^{\,3}}{24R^2} \text{ .... (13)}$$

Unified Zenith Delay Model (Wijaya, 2010)

The phenomenon of atmospheric delay has been modeled by Marini and Murray (1973) and Saastamoinen (1973). In 2004, Mendes and Pavlis created a new zenith delay model that was more accurate and could be applied to SLR wavelength (Satellite Laser Ranging). The formulation of Mendes and Pavlis (M-P) model uses the equation refractive index and density of water vapour from Ciddor (1996) as well as Ciddor and Hill (1999). This equation is commonly used in SLR with a wavelength of 0532 µm. The final formulation of hydrostatic zenith delay model (M-P) is:

$$\tau_{ho}^{z} = 24{,}16579 f_h(f_i) \times 10^{-6} \frac{P_s}{f(\phi, H)} \text{ ... (14)}$$

Wijaya (2010) created a unified zenith hydrostatic delay model (ZHD) from (M-P) models and dispersion refractivity group equation of Ciddor (1996) and resulted in the formulation:

$$\tau_{ho}^{z} = 0{,}1022 k_{dg}(f_i) \times 10^{-6} \frac{P_s}{f(\phi, H)} \text{ ...... (15)}$$

with:
τ_{ho}^{z} : *Zenith hydrostatic delay* (ZHD) for optic wave
$k_{dg}(f_i)$: dispersion formula for refractivity group
P_s : surface pressure (Pa)
ϕ : latitude of observation station
H : elevation of station (Km from sea level)

Where :

$$f(\phi, H) = 1 - 0{,}00266\cos 2\phi - 0{,}00028H \text{ .... (16)}$$

ZHD formulation of equation (14) and (15) is slightly different. Mendes and Pavlis (2004) created ZHD models by first derived density of dry atmosphere ρd as a function of pressure (P), temperature (T), and the vapour pressure (e). Then based on the ideal gas equation, they derived the total atmospheric density ρt and group refractivity based on modified dispersion formulation for wavelength 0532 µm. ZHD formulation by Wijaya (2010) indicates that equation by Mendes and Pavlis (2004) can be calculated in a more simple way. Besides, his formulation was prepared without simplifications and approximations. The values $k_{dg}(f_i)$ of dry air are not defined in the formula, so any dispersion formula can be used to determine ZHD, but this case is recommended to use the dispersion formulation of Ciddor (1996).

Zenith wet delay was integrated from Saastamoinen model (1973) and the definition of slant wet delay by Davis *et al*. (1985). The final formulation is obtained as follows:

$$\tau_{vo}^{z} = 10^{-6} k_{vg}^{*}(f_i) \frac{R_d}{4 g_m} e_s \qquad (17)$$

Where:

τ_{vo}^{z} : Zenith wet delay measurement of optical wave

$k_{vg}^{*}(f_i)$: groupped dispersion for water vapour

R_d : specified gas constant for dry air = 287.05 J/kg/K (Wallace dan Hobbs, 2006)

e_s : water vapour surface pressure

g_m : the acceleration due to gravity at the centre of vertical column of air (m/dt^2)

$$g_m = 9{,}784 \times f(\varphi, H) \qquad (18)$$

To estimate atmospheric delay at any elevation angle, mapping function (MF) is applied to map relationship between elevation and ray propagation. Marini (1972) stated that the MF could be formulated in the form of a simple *1/sin (∈)* which is the cutting of the equation:

$$m(\in) = \frac{1 + \frac{a_1}{1 + \frac{a_2}{1 + a_3}}}{\sin(\in) + \frac{a_1}{\sin(\in) + \frac{a_2}{\sin(\in) + a_3}}} \qquad (19)$$

with ∈ is the elevation angle of the rays, and the coefficients a_i *(i= 1, 2, 3)* were determined by least square fitting on beam curve depending on variation of meteorological parameters at the measurement location. MF is based on the assumption of hydrostatic equilibrium and symmetry azimuth and stating ratio of atmospheric delay at multiple elevation geometry, for example, delay to zenith direction.

Results and Discussion

TLS Range Measurement

Distance measurement results (initial data) are shown in Figures 3 to 5.These figures noted some data fluctuation. The measurement of Target A~50 m fluctuations occur at the beginning to 12th measurement, after that the measurement results are relatively stable. The results of measurements at distances of B~100 m and C~150 m fluctuations occur during the measurement time. Fluctuations of Target A~50 has the range from 1 mm (smallest) to 5 mm (largest), at B~100 m and C~150 m, the smallest is 1 mm and the largest is 2 mm. Fluctuations in A~50 m is relatively larger due to target position that is closer to the gas emission holes, while the positions of target B~100 m and C~150 m are further from the gas emission holes. The volcanic gas emission activity was continuing along the measurement process, some of gas particles passed in front of the target while laser beam hit the target. The average of measurement data can be seen in Figures 3 to 5 and Table 1.

The record of temperature, relative humidity, and air pressure (*thp*) data at base (TLS) and target is shown in Table 2. The temperature range at TLS base station is 15.3 - 23.6 °C, relative humidity 83 - 53%, and pressure of 785.1 - 783.2 hPa. The temperature range at target is 14.7 - 24.2 °C, relative humidity 87 - 43%, and pressure of 783.1 - 782.1 hPa. The range *thp* between TLS base station and target did not show any significant difference although *thp* at both places experienced fluctuation, but they give the same pattern.

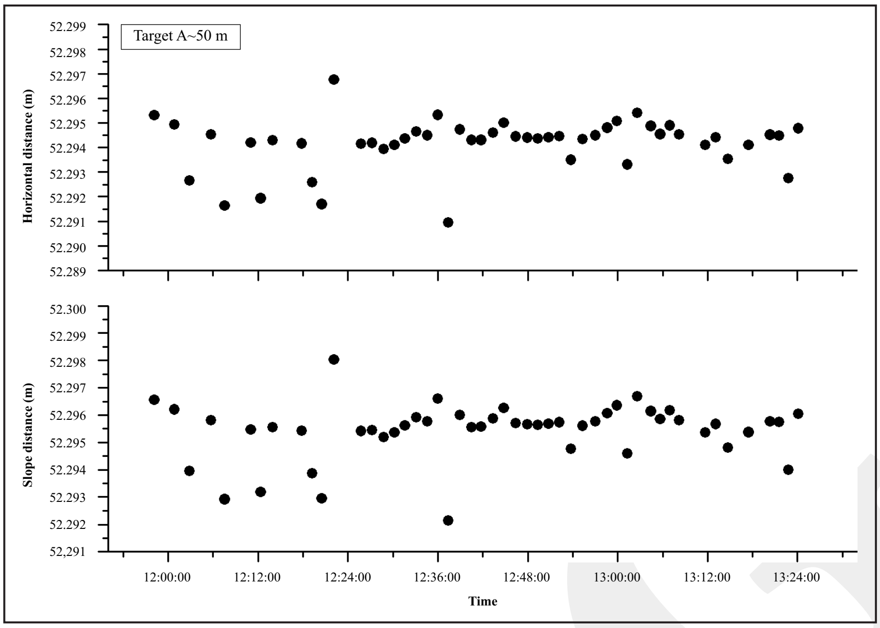

Figure 3. Horizontal and slope distances obtained by TLS measurement for Target A.

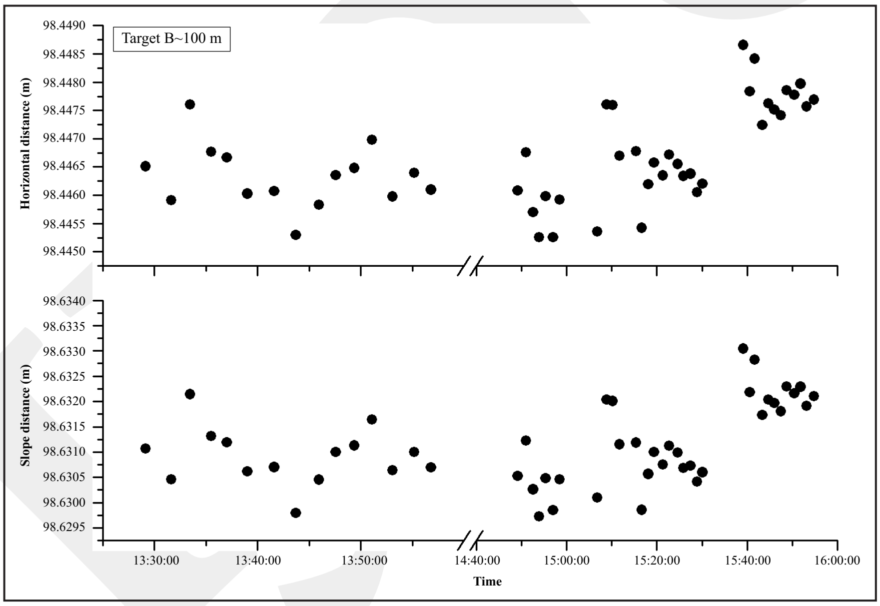

Figure 4. Horizontal and slope distances obtained by TLS measurement for Target B.

Corrected Distance and Comparison of Two Correction Models

The corrected distance using velocity and geometry correction model are calculated using Equation (5) until (13). The correction result is summarized in Tables 2 and 3 and Figures 6 and 7.

The comparison of initial measurement with velocity and geometry correction results (Figures 6 and 7) shows that for a distance of ~50 m the corrected distance is shorter.While for B ~100 m and C ~150 m, it shows longer distances. K1shows a significant value in each range, even reaching a fraction of cm at A~50m. However, K2 and K3 show a very small value, as summarized in Tables 3 and 4. These small values of K2 and K3 are interpreted due to the involvement of spheroid curvature variables (R, radius of the earth), while the distance measured in this study

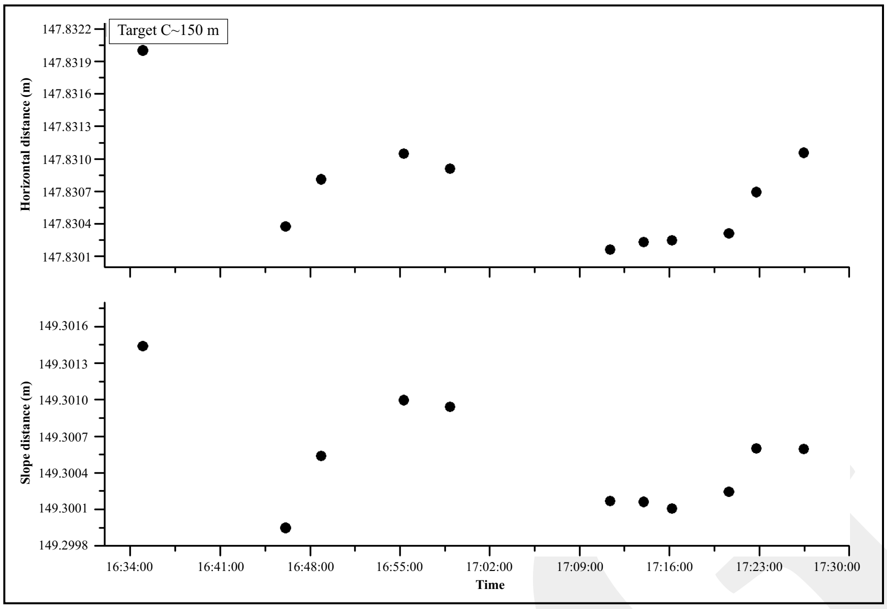

Figure 5. Horizontal and slope distances obtained by TLS measurement for Target C.

Table 1. Range of Measurement Result (Average)

Measured distance (m)	A~50		B~100		C~150	
	Horizontal	Slope	Horizontal	Slope	Horizontal	Slope
Average	52.29417	52.29543	98.44666	98.61088	147.83071	149.25317
σ	0.00104	0.00105	0.00086	0.00082	0.00054	0.00046

Table 2. Time of Measurement and *thp* Range at TLS Base Station and Target

Target	Time of measurement		*thp* at TLS			*thp* at target		
	Start	End	T (°C)	h (%)	P (hPa)	T (°C)	h (%)	P (hPa)
A	11:58:11	13:24:07	15.3 - 17.2	74 - 84	784.3 - 785.2	17.9 - 22	50 - 61	781.5 - 784.2
B	13:29:10	15:54:48	16.8 - 21.4	50 - 74	783.4 - 784	15.9 - 22.1	46 - 75	779.2 - 783.6
C	16:35:00	17:58:50	15.3 - 17.2	74 - 84	784.3 - 785.2	14.8-15.9	76 - 86	782.1 - 783.2

is relatively short. These small values cause K2 and K3 overly into K1 (ignored). In the further discussion, only K1 with ZHD model results which will be discussed.

ZHD correction model for TLS measurement distance applied uses Equation (15) to (19). The result of ZHD correction model can be seen in Table 5. Corrected distance for Target A shows a shorter distance for both correction model (K1 and ZHD), whileTargets B and C indicate the opposite pattern. In this case, ZHD model is considered to represent more actual size. Based on the difference value obtained from both correction model (Table 5), ZHD models show a consistent value than K1. In addition, the consistency of the difference is related to the distance between targets which are relatively the same, about 50 m.

Distribution of observation data is expressed by box plots on the right column of Figures 6 b, d, f, and 7 b, d, f. Targets A, B, and C show asymmetric distribution patterns, marked by elongated whisker on one side. Targets A and B show a distribution tendency of negative skewness, while target C shows a positive skewness. All distribution pattern of *d*, K1, and k shows the same pattern. This asymmetry indicates that there are outliers on data out of central tendency. Comparison of 2D position for each targets based

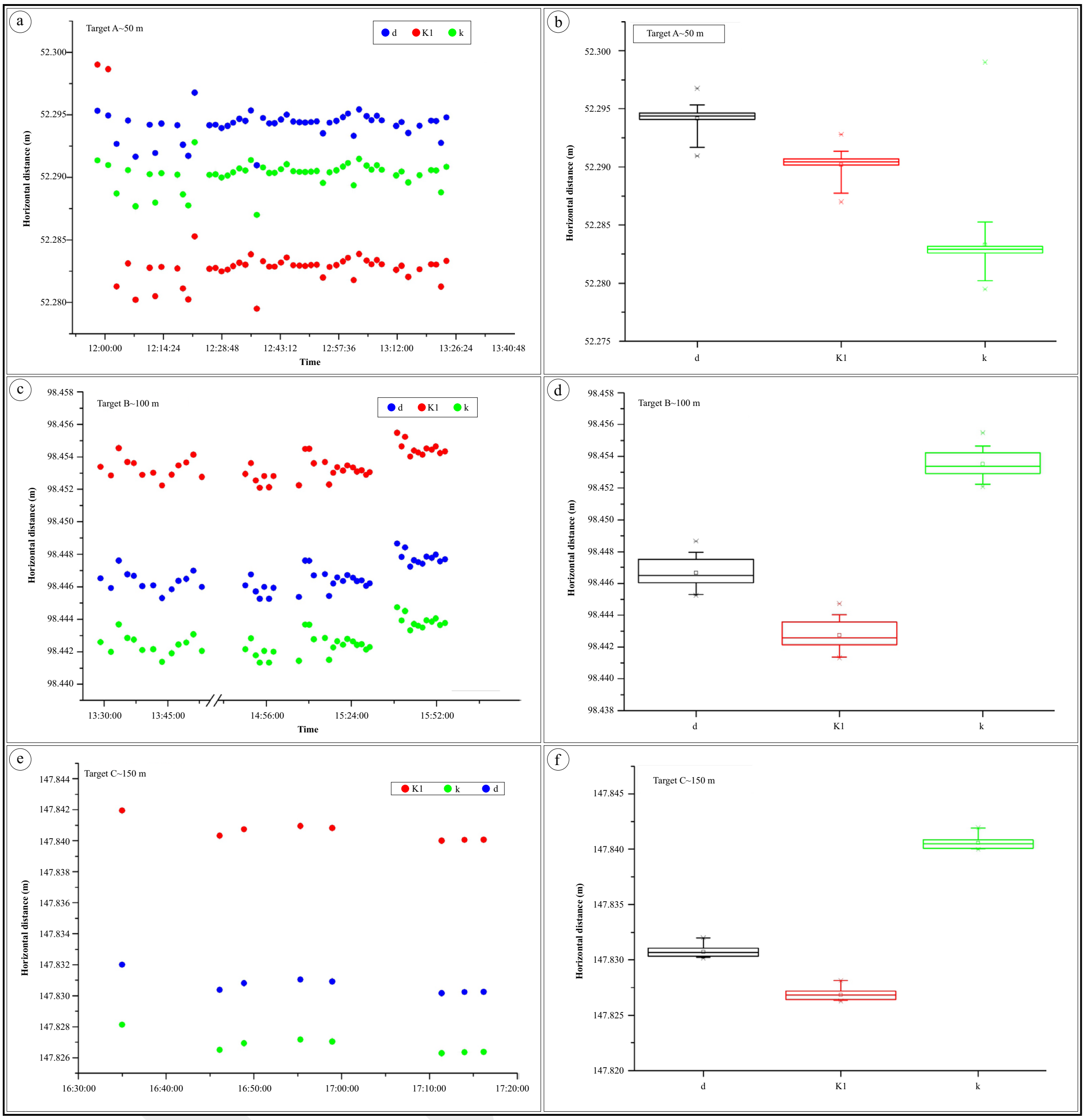

Figure 6. Comparison between initial horizontal distance (d), corrected distance using velocity correction model (K1), and ZHD model (k). Right columns (b, d, and f) show box plots for observation data.

on local coordinates is presented in Figure 8, while the 3D position in Figure 9. Both figures show that ZHD correction gives a smaller shift position than K1. For target A, the data tend to be more fluctuative at the beginning of measurement, possibly related to the phenomenon of false return (laser beam reflected by volcanic gas particles).

The difference between initial data (d) and corrected data (K1 and k) is presented in Table 6. The table shows that ZHD correction gives values close to the goal accuracy (based on Leica Scan Station C10 specification), which is 6 mm for position and 4 mm for distance. While K1 gives a higher value as well as positive and negative values. Thus, from an experiment using velocity and ZHD model, correction method using ZHD model is better than the fisrt one.

Figures 8 and 9 also note that ZHD correction (k) gives a shorter corrected distance which meets Fermat principle stating that the actual distances between two points measured by electromagnetic waves are those that have shorter travel times. In

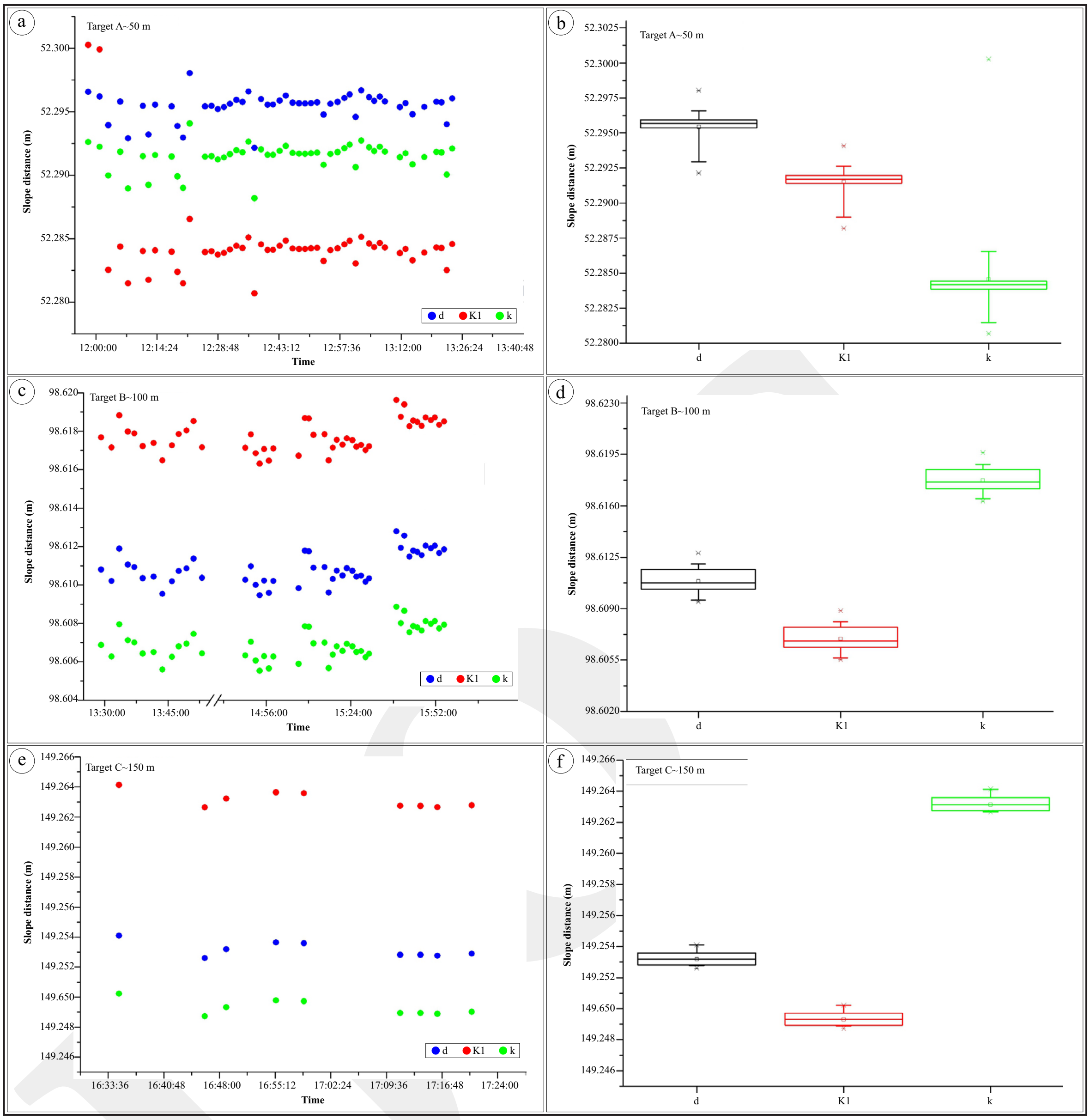

Figure 7. Comparison between initial slope distance (*d*), corrected distance using velocity correction model (K1), and ZHD model (k).

Table 3. Average of 1st Velocity (K1), 2nd Velocity (K2,) and Geometry (K3) Correction Result for Horizontal Distance

	A~50 m correction (m)	σ (m)	B~100 m correction (m)	σ (m)	C~150 m correction (m)	σ (m)
K1	-1.149×10^{-2}	0.00336	6.846×10^{-3}	0.00082	9.825×10^{-3}	0.00064
K2	-4.479×10^{-11}	0.00336	-1.714×10^{-10}	0.00082	5.020×10^{-15}	0.00064
K3	-1.092×10^{-7}	0.00336	-6.678×10^{-10}	0.00082	-5.867×10^{-13}	0.00064

Table 4. Average of 1st Velocity (K1), 2nd Velocity (K2), and Geometry (K3) Correction Result for Slope Distance

	A~50 m correction (m)	σ (m)	B~100 m correction (m)	σ (m)	C~150 m correction (m)	σ (m)
K1	-1.149×10^{-2}	0.00336	6.857×10^{-3}	0.00078	9.920×10^{-3}	0.00054
K2	-4.480×10^{-11}	0.00336	-1.722×10^{-10}	0.00078	5.069×10^{-15}	0.00054
K3	-1.092×10^{-7}	0.00336	-6.711×10^{-10}	0.00078	-6.038×10^{-13}	0.00054

Table 5. Comparison of Average Data: Initial Distance (d), Corrected Distance Using Velocity Model (K1), and Corrected Distance Using ZHD Model (k)

Target	d (m)	k (m)	K1 (m)	d-k (mm)	d-K1 (mm)
Horizontal distance					
A	52.29417	52.29021	52.28328	3.96	10.88
B	98.44666	98.44273	98.45350	3.93	-6.85
C	147.83071	147.82684	147.84057	3.87	-9.86
Slope distance					
A	52.29543	52.29147	52.28455	3.96	10.88
B	98.61088	98.60695	98.61774	3.93	-6.86
C	149.25317	149.24930	149.26313	3.87	-9.95

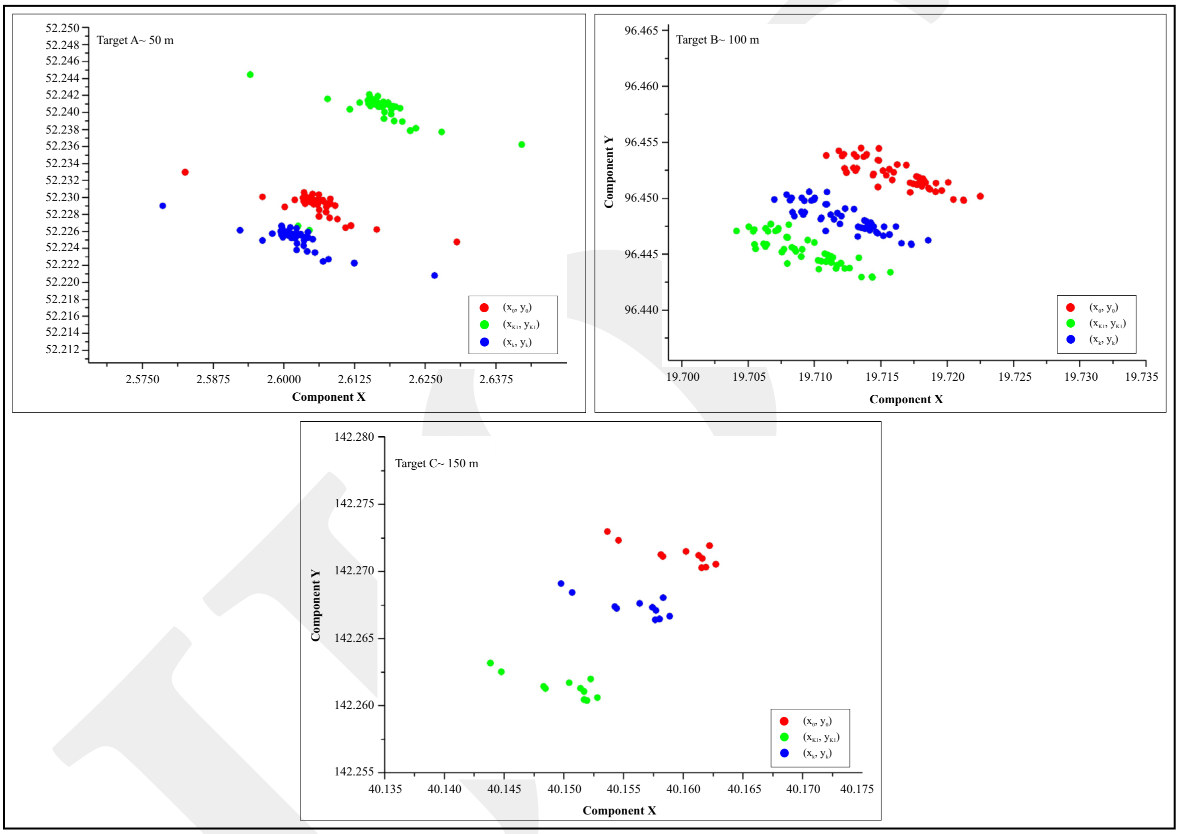

Figure 8. 2D position comparison of d (X_0,Y_0) red spot, K1 (X_{K1},Y_{K1}) green spot, and k (Xk,Y_k) blue spot.

addition, in terms of volcanic environment, the shorter corrected distance is in accordance with the phenomenon in Figure 2, where the distance measurement is influenced by the parameters of surface volcanic activity and the local atmospheric conditions.

RMS error of atmospheric delay correction calculation method can be estimated with pressure parameters (*P*), temperature (*T*), and the water vapour pressure (e_o) which can be formulated as follows (Abshire and Gardner, 1985):

$$\sigma_{datm} = \left[\left(\frac{\partial d_{atm}}{\partial P}\sigma P\right)^2 + \left(\frac{\partial d_{atm}}{\partial T}\sigma T\right)^2 + \left(\frac{\partial d_{atm}}{\partial e_o}\sigma_e\right)^2\right]^{1/2} \quad .... (20)$$

with σP, σT, and σe_o declare RMS on *P*, *T*, and e_o. Figure 10 shows the simulation results of a decrease in *P*, *T*, and e_o at elevation angle 5° up to 90°. From the figure, it is seen that P gives the greatest RMS. Simulation value of *P*, *T*, and e_o at 10° elevation and equation (9) gives the RMS value of 4.3 mm (Hulley, 2007).

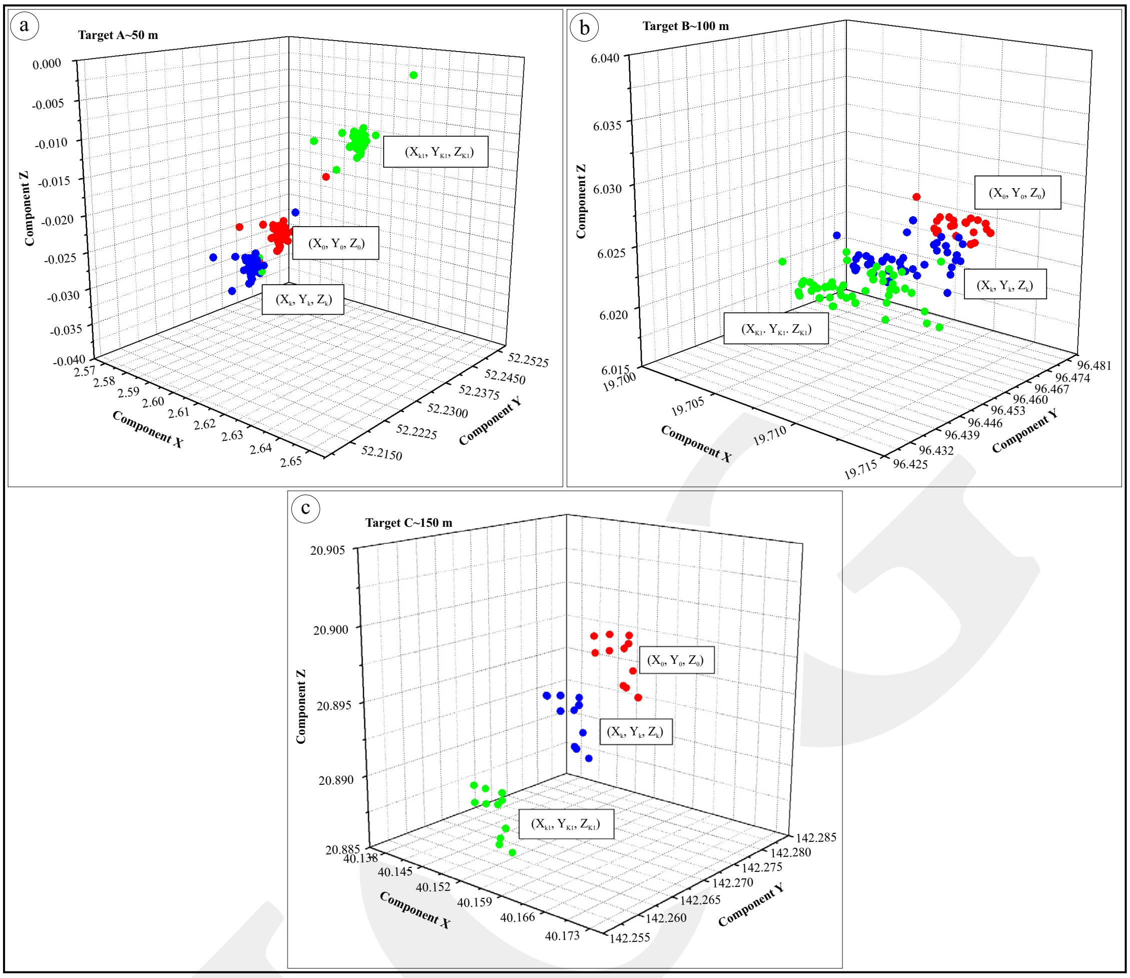

Figure 9. 3D position of d (X_0,Y_0,Z_0) red spot, K1 (X_{K1},Y_{K1},Z_{K1}) green spot, and k (X_k,Y_k,Z_k) blue spot.

Table 6. Comparison of Position Accuracy as a Result of Velocity Correction Model (K1) and ZHD Model (k)

Target	2D position accuracy (mm)		3D position accuracy (mm)	
	K1	k	K1	k
A	15.3877	5.5989	18.8461	6.8572
B	9.6817	5.5579	11.8577	6.8070
C	13.8418	5.4816	16.9527	6.7135

In this study, the elevation between TLS stands and Targets A, B, and C is very small (about 0.54°). If this value is simulated into Figure 10, the RMS value is greater than 4.3 mm. Table 7 shows that RMS value for all three targets on parameters of temperature, pressure, and water vapour pressure is in the range of 8.89 to 10.69 mm. Moreover, because of this small elevation value, it is assumed that there is no horizontal gradient effect. The differences in topographic height between TLS stand with targets A, B, and C are 0.4, 5.7, and 20.5 m, respectively.

Atmospheric delay model assumes that atmospheric conditions is in hydrostatic equilibrium. Irregularities related to turbulence, temperature changes, and vertical acceleration generated an error against the meteorological measurements (*thp*) itself. Saastamoinen (1973) estimated the maximum error of 1.5 cm at the elevation of 10°, while Hauser (1991) stated that for mountainous environment the error was smaller than 1 cm for elevation of up to 20°. In this study, the meteorological parameters are limited to *thp* variations in an active crater environment, whereas the effects of turbulence and atmosphere stratification layers of active crater surface is not discussed in detail.

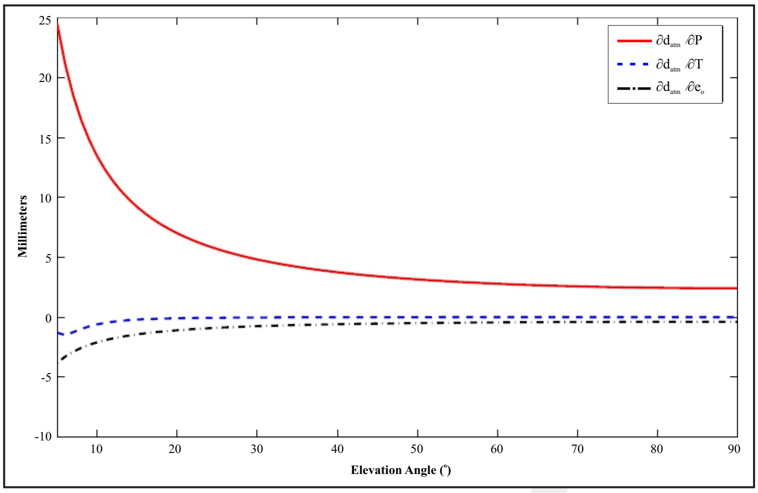

Figure 10. Atmospheric delay variation related to pressure, temperature, and water vapour pressure for elevation 5° to 90° (Hulley, 2007).

Table 7. RMS of Corrected Distance (using Atmospheric Delay Model) related with Parameter of Pressure (*P*), Temperature (*T*), and Water Vapour Pressure(e_o)

Target	Average			RMS (mm)
	T (C)	*e* (hPa)	P (hPa)	
A	20.06	12.98	783.29	10.61
B	18.80	13.51	782.09	10.69
C	15.27	14.32	782.76	8.89

Intensity of Volcanic Rocks

Tables 8 and 9 show the results of scanned volcanic rocks. For PBCB, there is a separation for dark (black-gray) and light (red-brown) parts to detect any differences on the intensity values.

The histograms in Figure 11 show that a darker colour has narrower ribbons of intensity values with peak values in the range of 0.15. While lighter colour has a wider ribbon and gives two patterns, one is in the range of <0.15 and the other at 0.15 to 0.2. Observing this histograms, it can be concluded that the darker colour has a more focused intensity value than the lighter one.

The intensity value histogram for the other rock samples can be seen in Figure 12. Figures 12 a, b, c, and d represent samples of fresh rocks, while images on the right columns (Figures 12 e, f, g, and h) indicate a group of weathered/altered rock samples (PCDB-1, GLBA-2, TPF, PCDB-2). From both groups of rock samples, the fresh rock provides intensity value histogram with clear dominant values and narrow band, while the weathered/altered rock has a wider intensity value range with several peak values.

To detect the correlation of mean intensity to scanned object properties, some graphs (Figures 13 to 15) are created based on megascopic ob-

Table 8. Summary ofVolcanic Rock Scanning Result

No.	Rock code	Rock type	#point clouds	Min - max intensity*)
1	PBCB (dark part)	Breadcrust bomb	6888	0.0761-0.3119
2	PBCB (light part)	Breadcrust bomb	3243	0.0743-0.2770
3	AKB	Breadcrust bomb	17323	0.0741-0.2240
4	PCDB-1	Cowdung bomb	5635	0.0753-0.2308
5	GLBA-1	Basaltic lava	4191	0.0797-0.2191
6	KKL	Andesitic lava	11525	0.0741-0.2360
7	GA	Andesitic lava	4298	0.1000-0.2345
8	TPF	Pumice	2047	0.1512-0.3361
9	GLBA-2	Basaltic lava	3024	0.0804-0.2267
10	PCDB-2	Cowdung bomb	4391	0.0753-0.1957

*) obtained with Cyclone v.8.

Table 9. Normalized Intensity Value of Scanned Volcanic Rocks

No.	Rock Code	Dominant intensity *)	Mean intensity	σ
1	PBCB (dark part)	0.1500-0.2000	0.1587	0. 0165
2	PBCB (light part)	0.0743-0.2770	0.1731	0. 0241
3	AKB	0.0741-0.2240	0.1679	0. 0195
4	PCDB-1	0.0753-0.2308	0.1693	0. 0236
5	GLBA-1	0.0797-0.2191	0.1653	0. 0079
6	KKL	0.0741-0.2360	0.1893	0. 0097
7	GA	0.1000-0.2345	0.1909	0. 0099
8	TPF	0.1512-0.3361	0.2410	0. 0193
9	GLBA-2	0.0804-0.2267	0.1853	0. 0159
10	PCDB-2	0.0753-0.1957	0.1563	0. 0100

*) obtained from histogram

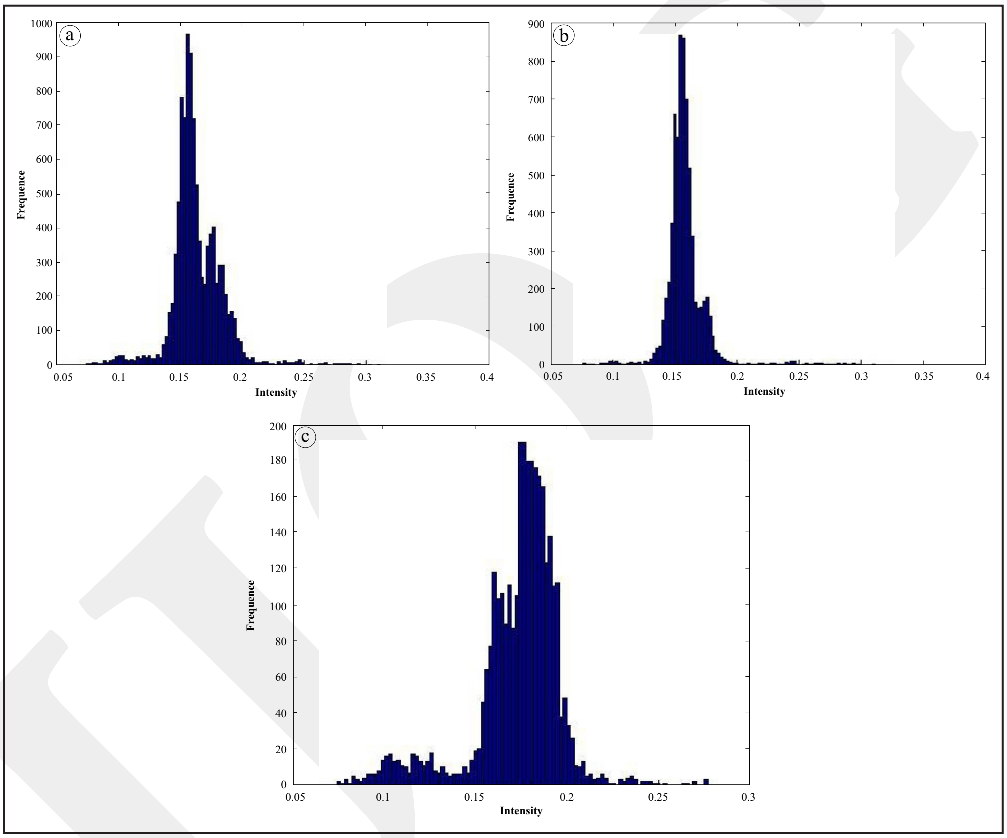

Figure11. Intensity value histograms of PBCB (breadcrust bomb). (a) All parts; (b) Dark part; and (c) Light part.

servations of these rocks including colour (dark to light), surface texture (coarse to fine), and mineral/crystal content (abundant to few).

All plots at Figures 13 to 15 show nonlinear patterns, but these graphs indicate that rocks with a lighter colour, smoother surface, and less crystal content, will give a higher intensity value. The range of mean intensity value for volcanic rocks in this study is from 0.16 to 0.24. This value range is lower than the other scanned objects measured from previous authors (Table 10).

Volcanic rocks in Indonesia generally consist of andesitic-basaltic type. Thus, it is assumed that the value of its intensity is in the range of 0.16 to 0.19 (represented by rock sample codes from PBCB up to GLBA-2). While TPF is more acidic (dacite) and very rarely produced by the recent volcanic eruption associated with caldera formation.

The preliminary result of volcanic rock intensity shows that the value is correlated with properties of rock surface, indicated by very clear colour parameters, surface roughness, and crystal

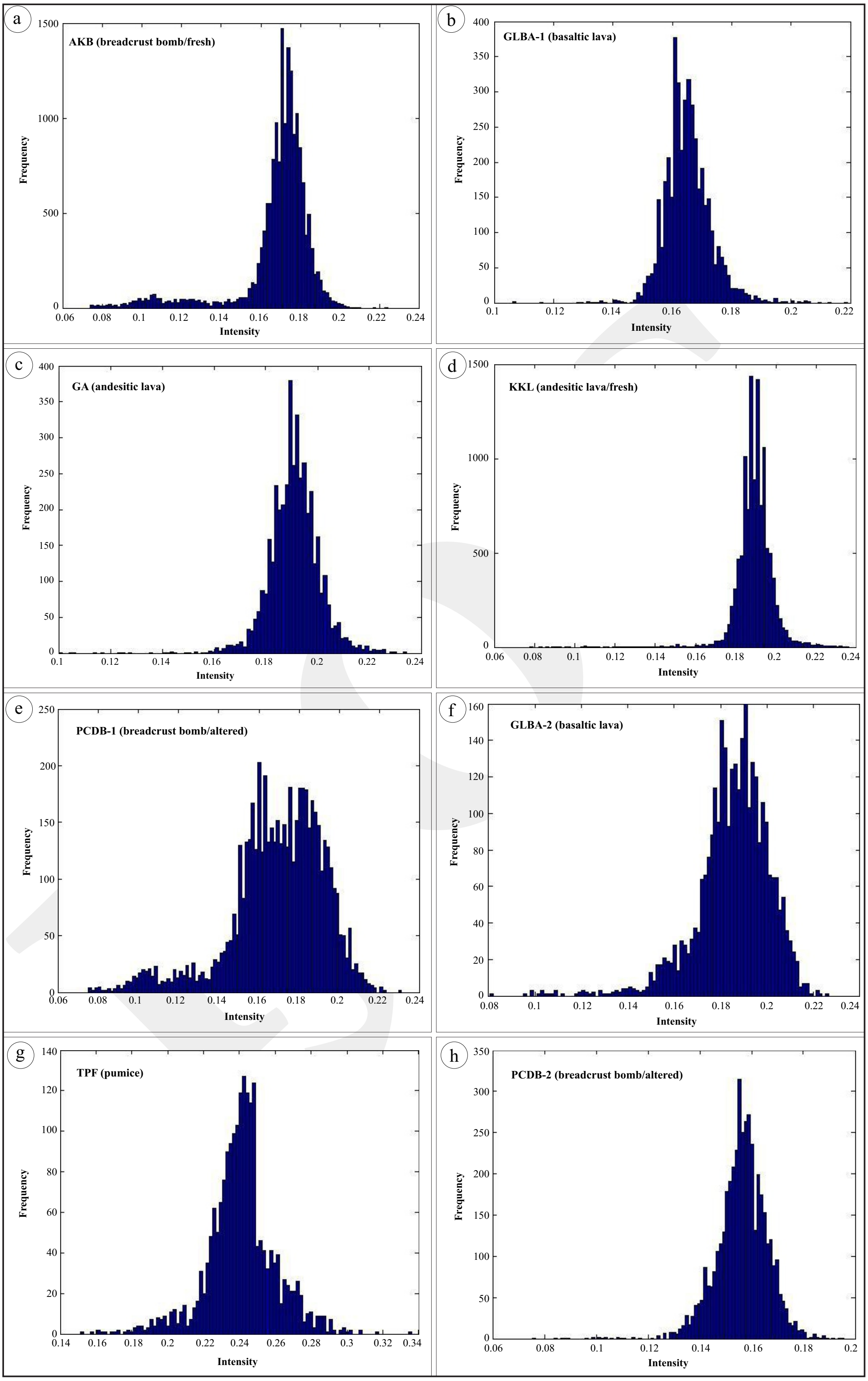

Figure 12. Histogram of intensity values for some volcanic rocks used in this research.

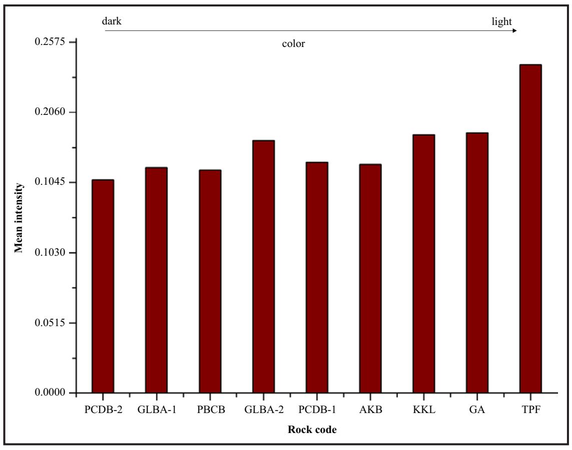

Figure 13. Mean intensity values of scanned volcanic rocks based on their colours.

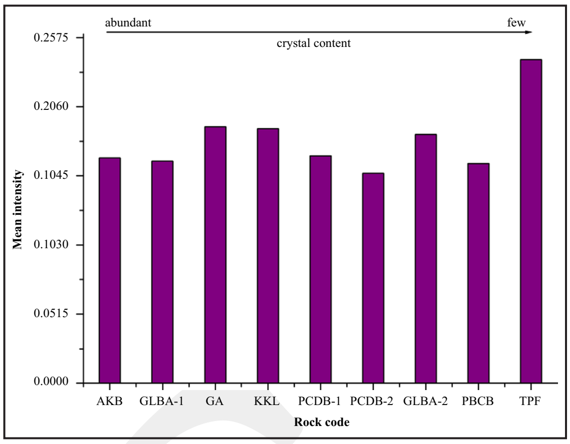

Figure 15. Mean intensity values of scanned volcanic rocks based on crystal contents/impurities.

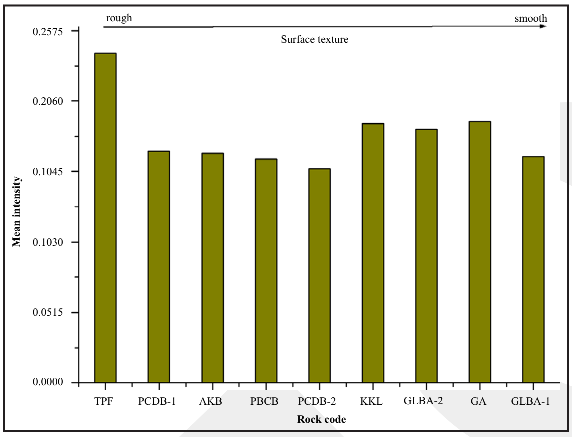

Figure 14. Mean intensity values of scanned volcanic rocks based on surface roughness.

content. This implies that volcanic rock with a lighter colour (lava dacite-andesite), smooth surface (non-vesicular), and less crystals content (nonporphyritic structure) will reflect a greater energy (intensity value) against TLS censor.The weathering/alteration degree of volcanic rocks affects the intensity value. Volcanic rocks that have been altered contain more minerals on its surface that serve as impurities. These preliminary assessments of intensity value of volcanic rocks show that segmentation/extraction of fresh volcanic rock outcrop can well be conducted, but for weathered/altered rocks it will be more complex. Therefore, it requires a detailed field survey to get more description.

The following discussion is about the effect of scanned object temperature with intensity value. Point cloud sampling on the intensity map was applied to thirteen areas that are considered to represent the range of temperature values. Sampling location and the range of temperature values can be seen in Figure 16. The mean value of intensity for each area is presented in Table 11. Figure 17

Table10. Mean Intensity Range of Volcanic Rocks Compared to Some Types of Scanned Objects

Haerani *et al.* (2016)			Litchi and Harvey (2002)		
No.	**Rock code**	**Mean intensity**	**No.**	**Objects**	**Mean intensity**
1	PBCB (dark part)	0.1587	1	Red brick	0.25
2	PBCB (light part)	0.1731	2	Limestone	0.39
3	AKB	0.1679	3	White granite	0.35
4	PCDB-1	0.1693	4	Coal	0.17
5	GLBA-1	0.1653	5	Concrete	0.30
6	KKL	0.1893	6	Marble	0.37
7	GA	0.1909	7	Basalt	0.30
8	TPF	0.2410	8	Laterite soil	0.26
9	GLBA-2	0.1853	9	White quartz	0.32
10	PCDB-2	0.1563			

Note: Scanning distance was reatively the same (~3 m);
All scanned objects are on dry condition)

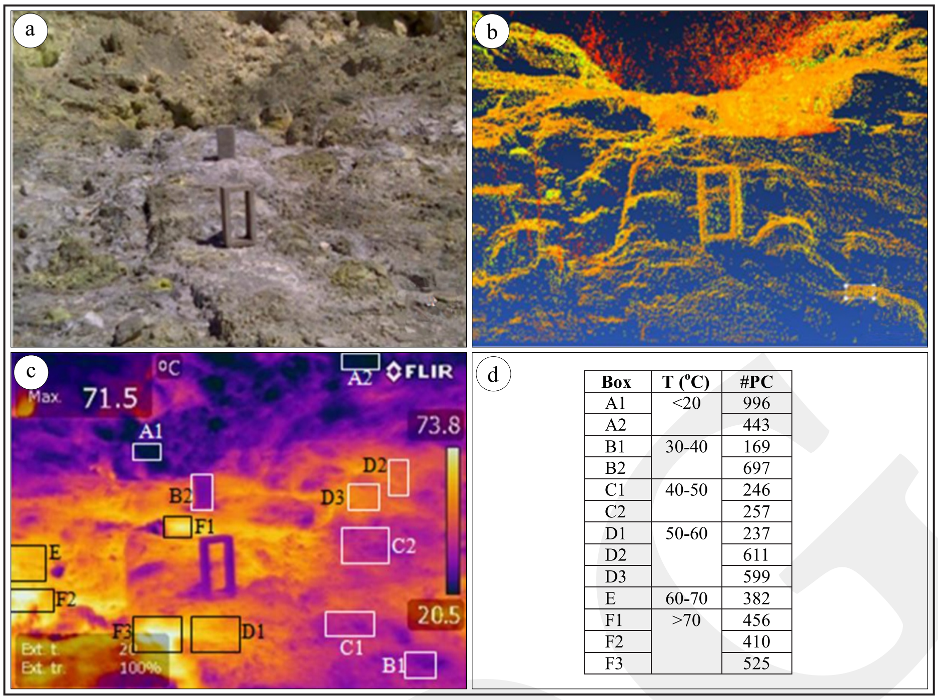

Box	T (°C)	#PC
A1	<20	996
A2		443
B1	30-40	169
B2		697
C1	40-50	246
C2		257
D1	50-60	237
D2		611
D3		599
E	60-70	382
F1	>70	456
F2		410
F3		525

Figure 16. Rock temperature observation around Papandayan Volcano crater and location of point cloud sampling. a). Condition of scanning spot. b). Intensity map as the result of scanning process.c). Result from thermal camera capture, and d).Explanation for each sampling area.

Table 11. Mean Intensity Value for Each Sampling Area

Box	T (°C)	Min - max intensity	Mean intensity
A1	<20	0.0743 - 0.3839	0.2722
A2		0.0861 - 0.7289	0.2572
B1	30 - 40	0.1649 - 0.2980	0.2356
B2		0.0900 - 0.4130	0.2070
C1	40 - 50	0.2116 - 0.2540	0.2313
C2		0.1959 - 0.2970	0.2236
D1	50 - 60	0.2113 - 0.3160	0.2368
D2		0.0841 - 0.5531	0.2233
D3		0.1268 - 0.3729	0.2184
E	60 - 70	0.0748 - 0.3729	0.2374
F1	>70	0.1657 - 0.3991	0.2537
F2		0.1251 - 0.3839	0.2394
F3		0.0756 - 0.3849	0.2438

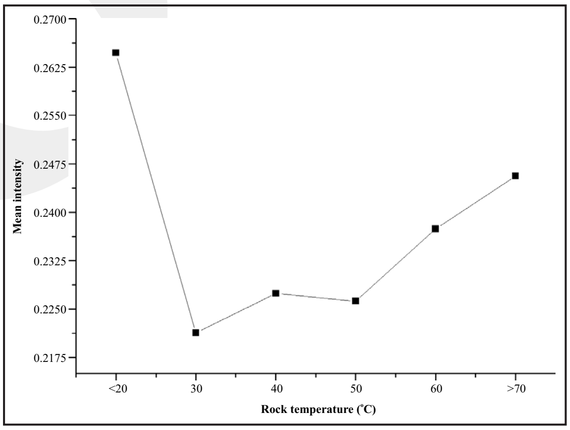

Figure 17. Plot of mean intensity value and temperature of the rocks. It shows a linier trend after 30°C.

shows a graph of relationship between the mean intensity with the temperature of the rocks.

Furthermore, Figure 16 shows that the highest temperature recorded by a thermal camera is 73.8°C and the lowest one is 20.5°C. For the calculation purpose, the limit of intensity value is taken at 70°<x<20° C. #PC indicates the number of point clouds (which contains the value of intensity) involved in the calculation. Plotting results of mean intensity value against temperature of rock show a positive linear pattern, where intensity values increase along with temperatures of rocks (Figure 17). However, on the rocks with temperature below 20°C, the intensity values show a higher level. It can be interpreted that within the temperature of 30°C on the object, scanning will start to affect the intensity value.

The maximum value of the measured temperature is ± 70°C. In practice, the temperature of emission gas holes in the surface can reach a higher temperature (200 - 600°C). Maata *et al.*

(1993) conducted a scan on a converter with temperatures of 1050° - 1400° C. The measurement results show that the received signal is increased by 28% in line with the increase in temperature. Thus, the pattern of increase in value of intensity against object temperature is linear.

Conclusions

Based on the data obtained, it can be concluded that atmospheric condition and surface activity of an active volcano crater (emission of volcanic gases) influence significantly into TLS range measurement. The application of first velocity correction K1 does not provide optimal results due to sensitivity of model to temperature changes, while the second velocity correction (K2) and geometry correction (K3) are not significant for a short distance. Correction using atmospheric delay model gives acceptable results, both in terms of correction magnitude value (consistent at 3.9 mm) or by dispersion phenomena. An atmospheric delay correction model gives a better accuracy in terms of 2D and 3D position.

Index refraction calculation using Ciddor formulation has already accommodated all parameters, but for applications in volcanic environments, it is necessary to find other alternative models or a new compiled model that involves dominant volcanic gas contents (N_2, CO_2, SO_2, H_2S, HCl, NH_3, and H_2O).

The brightness colour of the rock, crystal content, and roughness of rock surface affect the intensity value, in this case colour parameters are more dominant. The measurement of intensity values indicates that the volcanic rocks of andesitic-basaltic type derived from some volcanoes in Indonesia have intensity values ranging from 0.16 to 0.19.The temperature of the scanned object affects the mean value of the intensity recorded by TLS, in this case the mean value of the intensity starts to show the pattern of increase in temperature of 30° C. An increase in the value of intensity then has a linear pattern along with the object temperature.

Acknowledgments

The authors thank Geological Agency, Ministy of Energy and Mineral Resources of the Republic of Indonesia for funding this research; and Geodetic Laboratory, Faculty of Earth Science and Technology, Bandung Institute of Technology,which provided the authors with the equipment during the research.

References

Abshire, B., James and Gardner, S. Chester, (1985): Atmospheric refractivity corrections in satellite laser ranging. *IEEE transactions on geoscience and remote sensing*, GE-23, (4), July 1985. DOI: 10.1109/TGRS.1985.289431

Barrell, H. and Sears, J.E., 1939. The refraction dispersion of air for visible spectrum. *Philosophical Transactions of the Royal Society A: Mathematical, Physical and Engineering Sciences*, 238, p.1-64.

Birch, K.P. and Downs, M.J., 1994. Correction to the updated Edlen equation for the refractive index of air. *Metrologia*, 31, p.315-316. DOI: 10.1088/0026-1394/31/4/006

Boehler, W. and Marbs, A., 2006. *Investigating Laser Scanner Accuracy*. Institute for Spatial Information and Surveying Technology, University of Applied Sciences, Mainz, Germany.

Bonforte, A., Calvagn, F., Puglisi, G., and Sacareno, B., 2011. Terrestrial Laser Scanning (TLS) Over Volcanic Areas : Experiments on Vesuvius, Stromboli and Vulcano (Italy). *Geophysical Research, Abstracts*, 13, EGU2011-11657, 2011, EGU General Assembly 2011.

Ciddor, E.P., 1996. Refractive index of air: new equations for the visible and near infrared. *Applied Optics*, 35 (9), p.1566-1573. DOI: 10.1364/AO.35.001566

Ciddor, P.E. and Hill, R.J., 1999. Refractive index of air, 2 group index. *Applied Optics*, 38, p.1663-1667. DOI: 10.1364/AO.38.001663

Colombo, M. and Marana, B., 2010. Terrestrial laser scanning: how it works and what it does. *GIM International*, 24 (12), p. 17-20.

Davis, J.L., Herrig, T.A, Shapiro I.I, Rogers, A.E.E., and Elgered, G., 1985. Geodesy by radio interferometry; effects of atmospheric modelling errors on estimates of baseline length. *Radio Science*, 20 (6), p.1593-1607. DOI: 10.1029/RS020i006p01593

Edlen, B., 1996. The refractive index of air. *Metrologia*, 2, p.71-80.

Erickson, K.E., 1962. Investigation of the invariance of atmospheric dispersion with a long-path interferometer. *Journal of the Optical Society of America*, 52 (7), p.777-780.

Granthamn, J.W., Stargardt, C.D., Dungey, C., and Meidunas, E., 1997. Laser Radar in adverse weather. *Society of Photo-Optical Instrumentation Engineers (SPIE) Proceedings*, 3065, p.84-93.

Haerani, N., 2016.*Analisis dan pemodelan pengaruh lingkungan gunung api terhadap hasil pengukuran pemindai laser terestris (TLS)*. Disertasi.Program Doktor Teknik Geodesi dan Geomatika, Institut Teknologi Bandung.

Hauser, J.P (1991): Effects of deviations from hydrostatic equilibrium on atmospheric corrections to satellite and lunar laser range measurements, *Journal of Geophysical Research*, 94 (B8), p.10182-10186. DOI: 10.1029/JB094iB08p10182

Hofle, B. and Pfeifer, N., 2007. Correction of laser scanning intensity data: data and model-driven approaches. *ISPRS Journal of Photogrammetry and Remote Sensing*, 62, p.415-433. DOI: 10.1016/j.isprsjprs.2007.05.008

Hou, W. and Thalmann R., 1994. Accurate measurement of the refractive index of air. *Measurement*,13, p.307-314. DOI: 10.1016/0263-2241(94)90055-8

Hulley, G.C., 2007. Imroved refraction correction for *satellite ranging (SLR) by ray tracing through meteorological data.* Thesis (PhD), Faculty of Graduate School, University of Maryland, Baltimore, 160pp. Shaker Verlag Aachen.

Hunter, G., Pinkerton, H., Airey R.,and Calvari, S., 2003. The Application of A Long-range Laser Scanner for Monitoring Volcanic Activity on Mount Etna. *Journal of Volcanology and Geothermal Research*, 123 (1 - 2), p.203-210. DOI: 10.1016/S0377-0273(03)00036-2

Ingensand, H., 2006. Metrological Aspect in Terrestrial Laser Scanning Technology, Institute of Geodesy and Photogrammetry, ETH Zurich. *3rd IAG/12th FIG Symposium*, Baden.

Jones, L.D., 2007.*The Application of Terrestrial LIDAR to Volcano Monitoring - An Example from The Montserrat Volcano Observatory*. British Geological Surveys, Keyworth, Nottingham.

Jones, L.K., Kyle, P.R., Oppenheimer, O., and Frechette, J.D., 2015. TLS observations of geomorphic changes and varying lava lake levels at Erebus Volcano, Antartica. *Journal Volcanology and Geothermal Research*, 295, p.43-54. DOI: 10.1016/j.jvolgeores.2015.02.011

Jutzi B. and Stilla U.,2003. Laser pulse analysis for reconstruction and classification of urban objects. *ISPRS Archives*, XXXIV (3/w8), Munich.

Kaasalainen, S., Vain, A., Krooks, A., and Kukko., A., 2010. Topographic and distance effects in laser scanner intensity correction. Finnish Geodetic Institute, Department of Remote Sensing and Photogrammetry.*In*: Bretar, F., Pierrot-Deseilligny, M. and Vosselman, G. (eds.), *Laser scanning*, *IAPR*S, XXXVIII (3/W8).

Kaasalainen, S., Jaakkola, A., Kaasalainen, M., Krooks, A., and Kukko, A., 2011. Analysis of incidence angle and distance effects on terrestrial laser scanner intensity: search for correction methods. *Remote Sensing*, 3, p.2207-2221. DOI: 10.3390/rs3102207

Litchi, D.D. and Harvey, B.R., 2002. The effects of reflecting surface material properties on time-of-flight laser scanner measurements. *Symposium on Geospatial Theory, Processing, and Applications*, Ottawa, Canada.

Lichti, D.D.and Licht, M.G., 2006. Experiences with TLS modelling and accuracy assesment. *IAPRS,* XXXVI (5)*,* Dresden 25 - 27 September 2006.

Maata, K., Kostamovaara, J., and Myllyla, R., 1993. Profiling of hot surfaces by pulsed time-of-flight laser rangefinder techniques. *Applied Optics*, 32 (27)*,* p.5324-5347. DOI: 10.1364/AO.32.005334

Marini, J.W., 1972. Correction of satellite tracking data for an arbitrary tropospheric profile. *Radio Science*, 7, p.223-231.

Marini, J.W. and Murray, C.W., 1973. Correction of laser range tracking data for atmospheric refraction at elevations above 10 degrees. NASA Report, X-501-73-351.

Mendes, V.B. and Pavlis, E.C., 2004.High accuracy zenith delay prediction at optical wavelengths. *Geophysical Research Letter,* 31(L14602). DOI: 10.1029/2004GL020308

Mettenleiter, M., Hartl, F., Frolich, C., and Langer, D., 2000.Imaging Laser Radar for 3D-Modelling of Real World Environments. *Proceedings of International Conference on OPTO/IRS2/MTT*, May 9 - 11, Germany.

Owens, J.C., 1967. Optical refractive index of air; dependence on pressure, temperature and composition. *Applied Optics*, 6, p.51-59.

Peck, E.R. and Reeder, K., 1972.Dispersion of air. *Journal Optics Society of America*, 62, p.958-962. DOI: 10.1364/AO.6.000051

Pesci, A., Teza, G., and Ventura, G., 2008. Remote Sensing of Volcanic Terrains by Terrestrial Laser Scanner: Preliminary Reflectance and RGB Implications for Studying Vesuvius Crater (Italy). *Annals of Geophysics*, 51 (4)*,* p.633-653. DOI: 10.4401/ag-4455

Pfeifer, N., Dorninger, P., Haring, A., and Fan, H., 2007.Investigating Terrestrial Laser Scanning intensity data: quality and functional relations. *8th Conference On Optical 3-D Measurement Techniques*, p.328-337, Zurich, Switzerland.

Pfeifer, N., Hofle, B., Briese, C., Rutzinger, M., and Haring, A., 2008.Analysis of the backscattered energy in Terrestrial Laser Scanning data. The International Archives of the Photogrammetry. *Remote Sensing and Spatial Information Sciences,* XXXVII (B5), Beijing.

Quintero, M.S., Genechten, B.V., Bruyne, M.D., Ronald, P., Hankar, M., and Barnes, S., 2008. *Theory and Practice on Terrestrial Laser Scanning, Training Material Based on Practical Applications*, Vlaams Leonardo da Vinci Agenschap.

Reshetyuk, Y., 2006. Investigation of the influence of surface reflectance on the measurements with the terrestrial laser scanner Leica HDS 3000. Zeitschrift für Geodäsie, Geoinformation und Landmanagement 2006 (2), 96-103.

Reshetyuk, Y., 2009. Terrestrial laser scanning error sources, s elf-calibration and direct georeferencing. *VDMVerlag Dr. Muller*, Germany.

Rueger, J.M.,1990.*Electronic distance measurement. An Introduction*, 3rd totally revised ed., Springer Verlag, Berlin.

Saastamonen, J., 1973.Contributions to the theory of atmospheric refraction, in three parts.*Bulletin Geodesique*, 105, p.279-298.

Staiger, R., 2003.Terrestrial laser scanning technology, systems and applications. *2nd FIG Regional Conference*, Marrakesh, Morocco, December 2 - 5.

Tsakiri, M., Lichti, D.and Pfeifer, N., 2006. 'Terrestrial laser scanning for deformation monitoring'.*12th FIG Symposium*. https://www.fig.net/resources/proceedings/2006/baden_2006_comm6/PDF/LS2/Tsakiri.pdf

Vidyan, Y., Abidin, H.Z , Gumilar, I., and Haerani, N., 2013. Pemanfaatan metode TLS (Terrestrial Laser Scanning) untuk pemantauan deformasi gunung api. Studi kasus: kerucut sinder Gunung Galunggung, Jawa Barat. *Jurnal Lingkungan dan Bencana Geologi*, 4 (1),p. 49-69.

Voegtle, T., Schwab, I., and Landes, T., 2008. Influences of different materials on the measurements of a Terrestrial Laser Scanner (TLS). *The International Archives of the Photogrammetry, Remote Sensing and Spatial Information Sciences*, XXXVII (B5), Beijing, China.

Waggott, S., Clegg, P., and Jones, R., 2005. Combining Terrestrial Laser Scanning, RTK, GPS, and 3D Visualisation: Application of Optical 3D Measurement in Geological Exploration. *7th Conference on Optical 3-D Measurement Techniques*. Vienna, Austria. http://info.tuwien.ac.at/ingeo/optical3d/o3d.htm

Wallace, J.M. and Hobbs, P.V., 2006. *Atmospheric Science; An Introductory Survey* (2nd ed.). Academic Press.

Wijaya, D.D., 2010. *Atmospheric Correction Formulae for Space Geodetic Techniques*. Shaker Verlag Aachen.